Luminescent converter of solar light into electrical energy. Review

M.R. Kulish[1*], V.P. Kostylyov[1], A.V. Sachenko[1], I.O. Sokolovskyi[1], D.V. Khomenko[1], A.I. Shkrebtii[2]

[1]*V. Lashkaryov Institute of Semiconductor Physics, NAS of Ukraine,*
41, prospect Nauky, 03028 Kyiv, Ukraine
[2]*University of Ontario, Institute of Technology,*
Simcoe Street 2000 N, Oshawa, ON, L1H 7K4, Canada
*Corresponding author e-mail: n_kulish@yahoo.com

Abstract. We review a status of the research on conversion of solar energy into electricity by using the systems that split the solar spectrum with a set of luminescent concentrators. Influence of the luminophore choice (rare-earth elements, dyes, or semiconductor quantum dots) and their characteristics as well as the luminescence quantum losses, when the light quanta travel inside the optical waveguide formed by the luminescent concentrator, were analyzed. The methods to minimize these losses, including optimal converter design, were discussed. The choice of design with stacked luminescent concentrators was demonstrated. The design of the stacked luminescent concentrators with optimized parameters of the transparent matrix and semiconductor quantum dots was investigated.

Keywords: luminescence, luminophore, solar cells, efficiency, concentrator.

1. Introduction

Current researches on power generation by using photovoltaics are often aimed at single *p-n*-junction silicon solar panels. These panels, however, cannot utilize the total energy of sunlight (see Fig. 1 [1]). The bandgap of semiconductor material determines the fundamental limit, which defines how much energy of the sunlight can be converted into electrical energy. Thus, when the energy of photons is less than the semiconductor bandgap, they are not absorbed. In a Si cell, these losses can be as high as 19% (Fig. 1). For the photons with the energy above the gap, their excess energy ($h\nu - E_g$), where $h\nu$ is the photon energy and E_g – bandgap, is converted into heat, and therefore it is also lost (the so-called thermalization losses). In the Si solar cell, these losses can reach 33% (Fig. 1). A part of photogenerated carriers are lost during their separation by the *p-n*-junction, these losses can reach 15% (Fig. 1). Only 33% of the photons in the solar spectrum are available to be converted into electrical energy. As a result of the above losses, the theoretically attainable efficiency of the silicon solar cells cannot exceed 30% [2]. The maximum efficiency achieved experimentally is around 25% for AM1.5 [3].

The solar cell efficiency increase can be achieved by concentrating the photons incident on the input surface of the cell. When the light concentration equals to 92 suns, the single junction solar cell efficiency η reaches 27.6% [3].
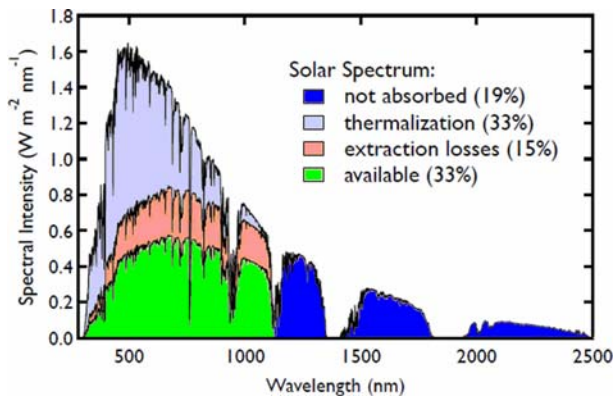
Fig. 1. Minimum losses for a silicon solar cell (bandgap of 1.1 eV) and where they occur in the solar spectrum (top line). These are the losses accounted for in the Shockley–Queisser limit and represent the upper limit for the single-junction solar cells made of bulk crystalline semiconductors. Thermalization represents the largest loss in this formalism, and it increases for the blue portions of the solar spectrum. See the text for an explanation of each loss [1].

A significant increase in the efficiency of sunlight conversion into electricity can be achieved by splitting the solar spectrum on spectral bands; each of them sends the light to a separate cell zone. There are two options for implementing this concept. In the first case, materials with a one *p-n*-junction are stacked in such a manner that the cell zone with the lowest bandgap is at the bottom and material with the highest bandgap is at the top. In particular, for such a structure with three *p-n*-junctions ($Ga_{0.5}In_{0.5}P/GaAs/In_{0.3}Ga_{0.7}As$) under AM1.5 conditions, the maximum efficiency for the non-concentrated light reaches 33.8%, and for the 81-sun concentration the efficiency $\eta = 38.9\%$ [4]. In [5], the record efficiency $\eta = 44.7\%$ has been reported in the structure with four *p-n*-junctions at 297 suns for AM1.5 conditions. In the technical realization of these structures the main difficulties are caused by the need to match the semiconductor lattice constants of the stacked semiconductors. For the second concept, the solar cells with different spectral sensitivity are placed laterally using a dispersion element that splits sunlight into bands. A prism, diffraction grating or set of interferential filters can be used as the dispersion element. Each solar cell is illuminated with a corresponding band of sunlight [6]. The maximum value $\eta = 43\%$ under AM1.5 has been achieved by splitting the solar spectrum into three bands and each band illuminates cell with multiple junctions. The first light band is transformed into electrical energy by two GaInP/GaAs *p-n*-junctions, the second band irradiates Si cell, the third one illuminates GaInAsP/GaInAs stack [7]. These structures can efficiently convert sunlight to electricity only at the normal incidence onto the photoconverter surface, and they cannot convert diffuse light into electrical energy. This is the main disadvantage of such structures. To

maximize the efficiency of these photoconverters, the tracking systems, which orient the panel to achieve the normal incidence onto the surface of the panel, are required.

The above disadvantages are not inherent to the Light Converter structures with Luminescence Concentrator (LCLC). LCLC operation is based on four mechanisms: (1) absorption of the light by the luminophore particles, (2) luminophore emission of the photons with energies lower than those of the absorbed photons, (3) transport of the fluorescent photons in a peculiar optical waveguide to the input surface of the solar cell, and (4) converting light into electricity by the solar cell. The advantages of such converters are the possibility of light concentrating at the input of the surface solar cells, the possibility of converting the scattered light into electrical energy, while the tracking systems for the solar panel orientation toward the sun is not required. In majority of the articles estimate the maximum efficiency η_c of the luminescent solar concentrator (LSC), it is done for the concentrator doped certain luminophore (mainly certain dye) (see, *e.g.*, [8, 9]). For the structure of a fluorescent concentrator doped with two dyes, the maximum efficiency achieved experimentally $\eta_c = 7.1\%$ [10]. The relatively low value of η_c is a consequence of the low efficiency of LSC, although it was theoretically shown that the quantum efficiency η_q of luminescent concentrators can be close to unity (according to [11] the maximum value $\eta_q = 99.7\%$), since the number of the light quanta absorbed by the luminophore should be equal to the number of fluorescent quanta.

Experimental LSC low efficiencies (less than ten percent) are caused by the fact that only a part of sunlight is able to create luminescent quanta, and there are luminescent quanta losses in the concentrator. There are two ways to improve LCLC efficiency. 1) Minimize all possible losses of the quanta in the LSC with its efficiency close to unit and to match the spectral luminescence band with that of maximum efficiency of the solar cell. 2) Form a stack of the LSC and achieve the current matching between the solar cells, which creates a peculiar photoconverter with luminescent splitter of the solar spectrum.

The purpose of this work is to find ways of forming stacked LSC, attached to each LSC solar cells. To achieve it, we have to: 1) determine the optimal number of stacked concentrators, 2) minimize the loss of light in each LSC plate and in stacked LSC, 3) determine the design of each plate in LSC and of the whole stacked LSC.

To attain this result, we consistently considered: 1) principle of LSC operation and identified all types of light quanta losses as well as the ways to minimize them, 2) analyzed the luminophore properties and determined the type of the optimal luminophore, 3) properties of the matrix LSC and found optimal geometry of both the individual LSC matrix and stacked LSCs.

2. Luminescent photoconverter

As a luminescent photoconverter, we mean stacked concentrators with the solar cells, attached to each concentrator (Fig. 2). For example, we demonstrate the principles of such photoconverter operation by using three stacked LSCs. The luminophore located at the top LSC plate absorbs only the high energy part of the solar spectrum. As a result of absorption, luminophore molecules transfer to the excited state. Transition of the molecules to the ground state is accompanied by emission of luminescent photons in a narrow energy band. These photons propagate in the plate as in a peculiar optical waveguide and eventually get transferred to the lateral side of the plate, which is the input surface of the solar cells. The solar cells convert energy of the luminescent quanta into the electrical one. Light and fluorescent quanta that are not absorbed by the highest concentrator pass into the second LSC plate. There, luminophore molecules absorb less energetic part of the solar spectrum and emit luminescent quanta in the second narrow luminescence band. Luminescence quanta in the optical waveguide are transmitted to the input of solar cells attached to the middle LSC plate and are converted into the electrical energy. The rest of the solar spectrum (not absorbed in the upper concentrators) reaches the bottom LSC plate, where the luminescent molecules absorb the remaining solar quanta and emit the luminescent quanta in a narrow band. Fluorescent photons transferred to the solar cell are converted into the electrical energy again.

It should be noted that such stacked LSC are the splitter of the solar spectrum into a set of spectral bands. If each input area of the LSC plate is much larger than the area of end faces with the solar cell attached, the ratio of these areas determines the value of the light concentration. Therefore, the ideal LSC is simultaneously the concentrator of the solar energy and the solar spectrum splitter. To estimate the maximum possible efficiency of such photoconverter, we have to determine the losses both in the stacked LSC and in solar cells, as well as identify ways to minimize these losses. Next, one has to simulate the real and idealized fluorescent phototransducer. Let's start with the losses in a separate LSC.

3. Losses of the luminescent quanta in LSC

We consider first a luminescent concentrator as a plate (in the simplest case of the rectangular shape) transparent to the sunlight and doped with a luminophore (consisting of rare-earth ions, or dyes, or quantum dots) with no solar cells attached to plate (see Fig. 3). Sunlight incident on the input surface plate is denoted as (1), small part of it (2) is reflected from the plate and lost. Another part of the photons passes through the plate without absorption (3) and is lost. Part of the photons is absorbed by absorption centers (4) of the plate and is emitted by the fluorescent centers (5). Each luminescent center radiates photons in all directions (6). If the absorption and luminescence spectra overlap, the fluorescent photons can be reabsorbed (7) and excite the
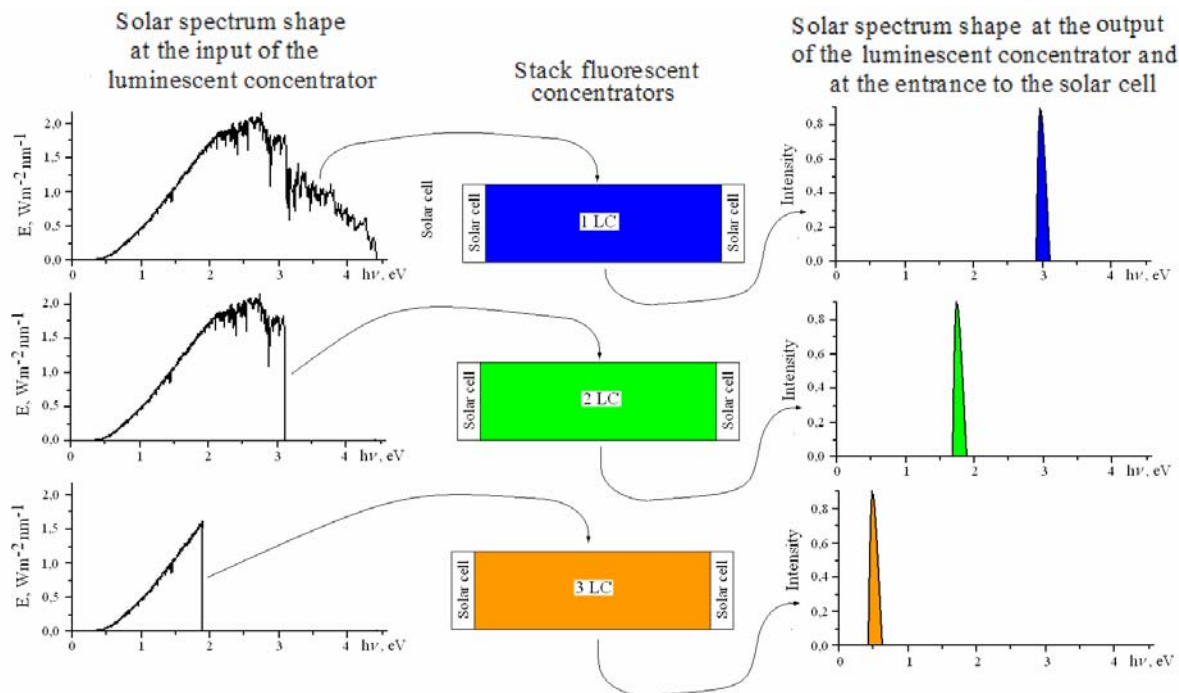

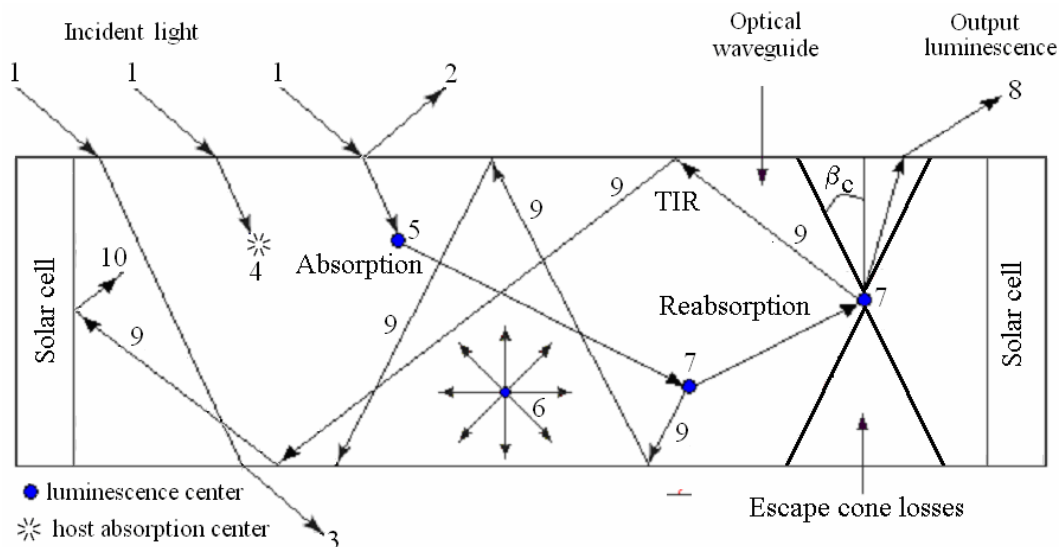**Fig. 2.** Illustration of LCLC operation.

Fig. 3. Cross-section of the luminescent solar concentrator with a schematic representation of the loss of sunlight photons. Light that enters the LSC is absorbed by luminescent centers. Each luminescent center emits photons in all directions. Fluorescent photons that emit under angle smaller than the critical one leave the matrix. These photons are concentrated in the cones marked by the heavy lines. Fluorescent photons that are emitted at an angle larger than the critical one, spread into the optical waveguide. They can be reabsorbed either directly or after total internal reflection and surface transport to the input solar cells face.

luminescent centers that generate quanta of luminescence. The part of luminescent photons that are spread at the angles below the critical angle β_C (8) leaves the plate. Those photons that are spread at angles above the critical one β_C (9) are reflected from the surface of the plate and travel inside the optical waveguide to the end surfaces. When the refractive indices of the plate and solar cell are different, the part of photons is reflected back into the waveguide (10). At all the stages of interaction of the light inside the plate, light quanta can be additionally lost.

3.1. Reflection losses

The intensity of light I_{tran} passing through the front surface of the concentrator is

$$I_{tran} = (1 - R)I_0, \qquad (1)$$

where R is the reflection coefficient, I_0 − intensity of the incident light on the front surface of the plate. The value of the losses of light in this case is $\eta_{tran} = I_0 R$. When the incident light is normal to the plate, then the reflection coefficient R can be estimated by the formula

$$R(\lambda) = \left(\frac{n(\lambda) - 1}{n(\lambda) + 1} \right)^2, \qquad (2)$$

where $n(\lambda)$ is the refractive index of the material of the plate.

To reduce the reflection losses, one can either manufacture the plates using low refractive index material or apply deposit an antireflecting film onto the front surface of the plate. However, as it will be shown below, the use of the antireflecting film is inappropriate.

3.2. Transmission losses

These losses are caused by the limited absorption band of the luminophore. Reduction of these losses can be achieved by using as much as possible LSCs in the stack and by setting high luminophore concentrations, which absorb all sunlight. Detailed analysis of the properties of luminophore will be made below.

3.3. Luminescence quantum yield

In the concentrators, luminophore converts sunlight of particular spectral range into narrow luminescence band by luminescent centers that are uniformly distributed inside the plate. Luminophore emits photons in a lower energy region as compared to the absorption spectrum range. This process is characterized by the luminescence quantum yield (η_L), which is a ratio of the concentration of the emitted photons N_L to the concentration of the absorbed photons N_a.

$$\eta_L = N_L / N_a. \qquad (3)$$

It is necessary that in each concentrator the η_L value is close to unity.

Energy of the fluorescent photons usually differs from the energy of absorbed photons. The energy losses are caused by the Stokes shift, can be approximately characterized by η_{st}, equal to

$$\eta_{st} = \frac{\Delta h\nu_L}{\Delta h\nu_{ab}}, \qquad (4)$$

where $\Delta h\nu_L = \Delta h\nu_{L\,max} - \Delta h\nu_{L\,min}$ is the width of the luminescence band at the 0.1 level, $h\nu_{L\,max}$ and $h\nu_{L\,min}$ are

the maximum and minimum energies of the luminescence quanta at 0.1 level, $\Delta h\nu_{ab} = \Delta h\nu_{ab\ max} - \Delta h\nu_{ab\ min}$ is the bandwidth of the light absorption by luminophore, $h\nu_{ab\ max}$ and $h\nu_{ab\ min}$ are the maximum and minimum energies of the quanta absorbed by the luminophore. The energy losses can be minimized by narrowing the fluorescent band as much as possible and by simultaneously increasing the absorption bands in a maximum possible manner.

4. Luminophores

The properties of luminophores determine substantially the efficiency of solar concentrator. When analyzing perspectives of using luminophores for doping concentrator plates, the following criteria have to be used [12]:

1. Absorption band should be broad and not striped to fully use solar energy containing in that band.
2. Luminophore absorption coefficient should be high enough for complete absorption of photons.
3. Luminescence band must be narrow as compared to the absorption band. It is desirable that the distance between the bands was the maximum possible.
4. The quantum yield of luminescence must be high, ideally close to unity, and temperature independent.
5. The overlap of the absorption and luminescence spectra should be minimal. Ideally, the spectra should be completely non-overlapping, that is the self-absorption of luminescence can be neglected.
6. The luminophore emission band must coincide with the area of the maximum external quantum yield of the solar cell.
7. Photostability should be kept unchanged for a long time, ideally within 30-50 years, which is close to the lifespan of solar panels.
8. Thermal resistance should be high, preferably above 400 K.
9. The cost and toxicity of the luminophores should be minimal.

An analysis of the luminophores properties is necessary to decide which ones are the best suited to satisfy the above criteria. In the analysis, provided below, the known luminophores are divided into three following groups: (1) rare earth atoms, (2) organic dyes and (3) quantum dots.

4.1. Rare-earth atoms and complexes

Ions of the rare-earth lanthanides group elements can be used as the luminophore in fluorescent concentrators. This includes atoms of such metals as erbium (Er), neodymium (Nd), samarium (Sm), europium (Eu), praseodymium (Pr), terbium (Tb), holmium (Ho), thulium (Tm), and ytterbium (Yb) as well as the atoms of transition metals such as chromium (Cr), titanium (Ti), vanadium (V) associated with the relevant complex. In the trivalent form, the lanthanides basically are stable. Ions of the lanthanides group have the

electron configuration $[\text{Xe}]4f^n5s^25p^6$, where n varies from 0 to 14. Partially filled 4f inner shell is responsible for the characteristic optical properties of the lanthanides. The number of configurations for the n electrons averaged over 4f orbitals is numerous. They determine the energy spectrum of the rare-earth elements, known as Dike diagram (Fig. 4) [13]. A characteristic feature of the energy spectrum of these metal ions is their discrete nature (Fig. 4). As the result, both the absorption and luminescence spectra of the ions are narrow-band, see, *e.g.*, the absorption and emission spectra of Nd^{3+} ions (Fig. 5) [14]. As shown in Fig. 5, the absorption spectrum of Nd^{3+} ions contain numerous peaks in the 300…900-nm range, which correspond to the transitions from $^4\text{I}_{9/2}$ ground state of the ion to different excited states.

The emission spectrum contains three peaks with the maxima at 880, 1064 and 1330 nm (not shown in the figure) with 75% of emissions originating from the main peak at 1064 nm. The emission goes from the $^4\text{F}_{3/2}$ excited state. Narrow-band absorption and luminescence spectra are typical for all rare-earth elements (see, *e.g.*, [9, 15-17]).

The main advantages of the matrices doped with rare-earth elements are as follows: 1) high internal quantum yield of luminescence, close to 70…100% [14], which also includes transitions in the infrared region; 2) Stokes shift of the luminescence is large (see, *e.g.*, Fig. 5). Due to this, the reabsorption can be neglected; 3) band of the luminescence is narrow; 4) photostability of rare-earth elements is high. These parameters remain unchanged over hundreds of years.

The main disadvantages of the matrix doped with metal ions are as follows: 1) Absorption bands of the rare-earth ions are numerous and narrow. 2) The absorption coefficient is low, so the thickness of the matrix doped with rare-earth elements should be significant, and high concentrations of rare-earth elements should be used for doping. This often leads to concentration quenching of the luminescence. 3) Correlation of the appropriate absorption band of the rare-earth ions with the range of maximum solar cells efficiency is difficult to achieve. 4) Technology of the matrix synthesis with rare-earth ions and transition metals are complex and expensive. 5) Selection of the ions of rare-earth metals is limited.

To achieve the maximum efficiency of solar energy conversion into the electrical energy, a rare-earth doped plate that completely absorbs the light from the corresponding spectral range is required. One way to implement this is to dope the plate with several rare-earth ions such as, for example, Nd or Yb [14]. However, in this case, the absorption spectrum contains regions with low absorption coefficients.

Expanding the absorption spectrum can also be achieved through formation of complexes of rare-earth ions or transition metal atoms. Usually such a complex contains rare-earth ion (which serves as an acceptor) related energetically with other metal ion or rare-earth
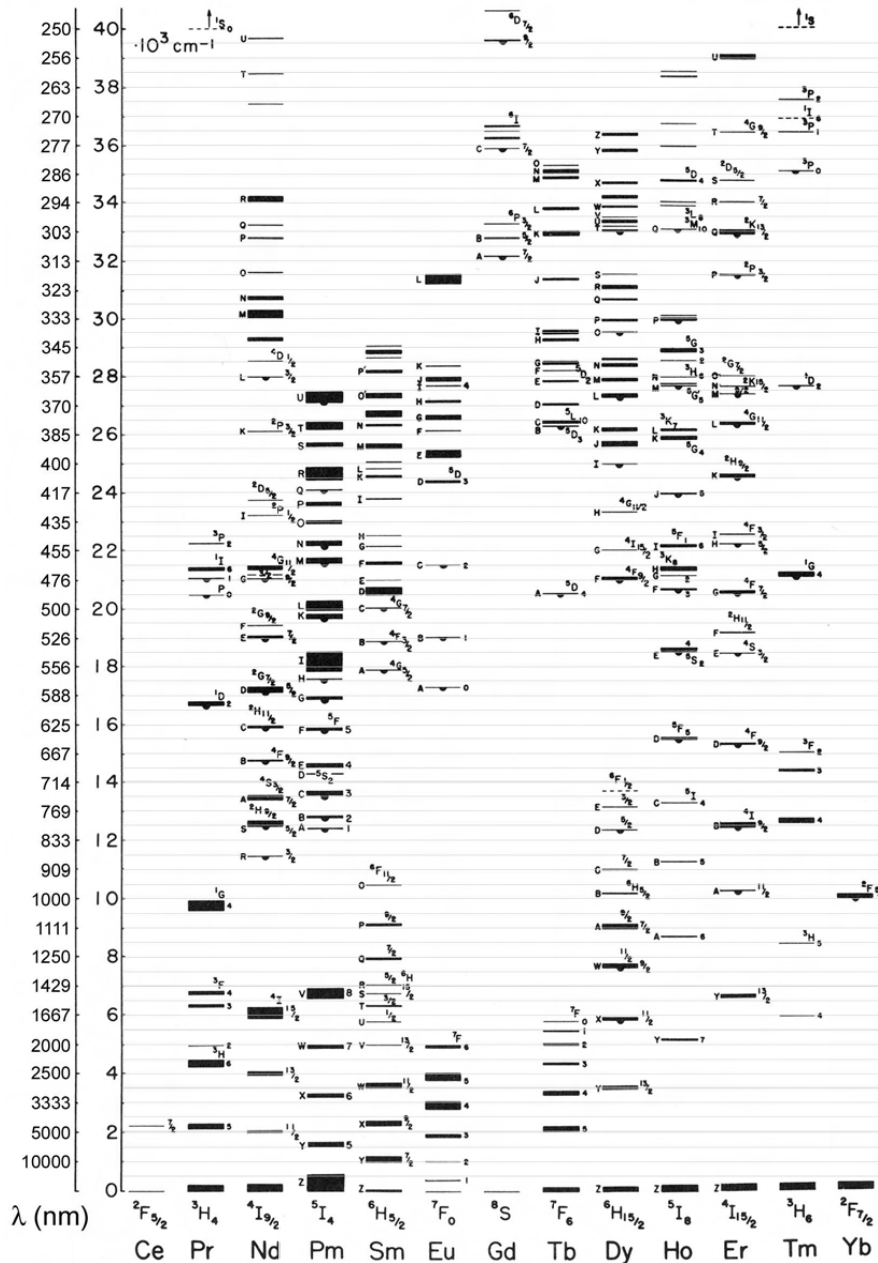
Fig. 4. Energy-level digram for RE^{3+} ions doped into the crystal LaCl$_3$ (after Dieke [13]). The first axis on the left represents the emitted photon wavelength from a given multiplet to the ground state only. The second axis on the left represents the energy (cm^{-1}) of the $^{2S+1}$L$_J$ level [13].

metal or transition metal ion (it serves as a donor). Typically, the acceptor is surrounded by the organic ligand. One example of such complex is shown in Fig. 6a [18, 19]. The light is absorbed by both the ligand and the rare-earth ion. The energy absorbed by the donor is not emitted but rather is non-radiatively transferred to the acceptor. As a result, the absorption spectrum of the complex becomes wider as compared to the absorption spectrum of the rare-earth elements (see Fig. 6b). For the efficient energy transfer from the donor to the acceptor, the maximum overlap of these absorption spectra is required.

Depending on the design, the energy transfer in the complex occurs through the dipole-dipole mechanism (so-called Förster mechanism [20], the energy is usually transferred from a single metal ion to another) or by the energy exchange mechanism by Dexter [21]. Structures of different types of ligands and complexes are described in many papers (see, *e.g.*, [22]). According to the authors of [23], the complex Eu (TTA) 3dpbt absorbs only 7.6% of the solar spectrum. Note that, in the field of transparency of the absorption spectrum of the ligand complexes, there are narrow absorption bands that are representative for rare-earth elements.
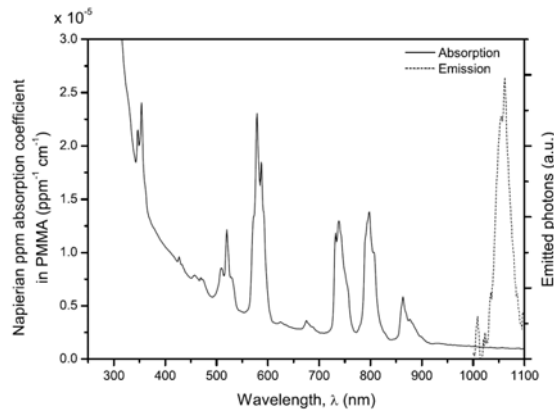
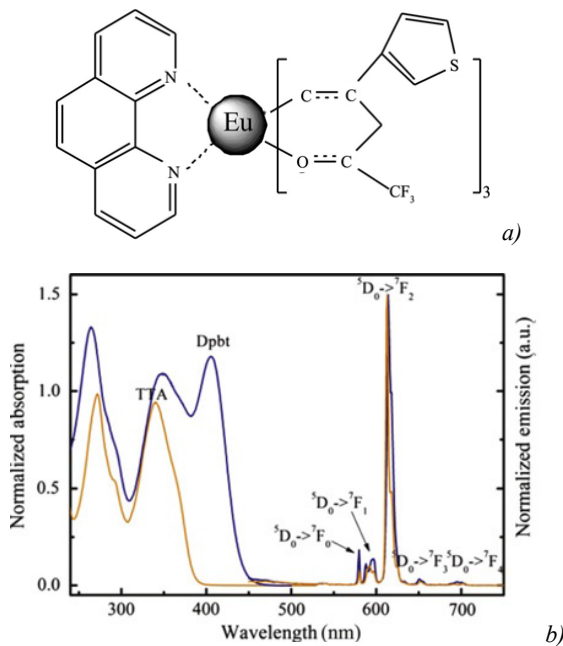**Fig. 5.** Absorption (solid) and emission (dashed) spectra of NdF$_3$ [14].

Fig. 6. The molecular structure of Eu (TTA) 3phen complex (a) [18] and (b) absorption and luminescence spectra of such complex systems [22].

Fig. 7. Visible (a) and near infrared (b) dye absorption and emission spectra (normalized) [14].

4.2. Organic dyes

The number of different organic dyes is huge. The absorption and luminescence spectra of most dyes lie in the visible and near infrared region [24, 25]. This is demonstrated in Fig. 7, which shows the absorption and luminescence spectra of several dyes [14]. Typical for the absorption spectra is that they are striped, and a significant overlap of the absorption and luminescence spectra occurs. The extent of the absorption bands of individual organic dyes is around 100 nm (Fig. 7) and usually covers from 10 to 15% of the area of the visible spectrum [12]. Therefore, to absorb the maximum number of photons, mixing the several dyes is necessary, which in many cases leads to the luminescence quenching.
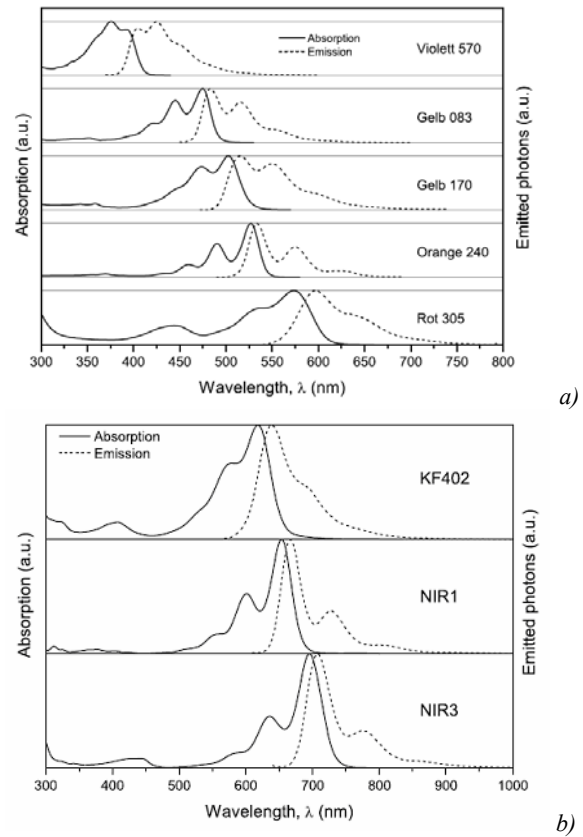
When the several dyes are inserted into the plate, the set of absorption spectra forms a broad absorption band. Short-wave photons transfer solar energy to the dye through cascade that generates photons with longer wavelengths. In this case, the efficiency of the luminescence concentrator is determined by the luminescence quantum yield of the dye that generates light in the long-wave range of the spectrum.

Luminescence quantum efficiency depends on the wavelength of the emission of dyes (Fig. 8). Fig. 8 shows that the longer the wavelength, the lower the quantum yield is. Dyes with the quantum yield of luminescence $\varphi \approx 1$ emit in the range below 600 nm. From 600 to 700 nm quantum yield dyes averages to $\varphi \approx 0.6$, from 700 to 800 nm, it drops to $\varphi \approx 0.4$ and beyond 800 nm range the quantum yield is reduced to its minimum $\varphi \approx 0.2$ [12]).

Dyes degrade and have a limited lifetime. The investigation of Violett 570 dye [12] has demonstrated that the intensity of luminescence PMMA doped dye samples is reduced to 50% from its initial value after exposure for two years. Incidentally, the value of the degradation is strongly dependent on the base polymer and exposure conditions. Obviously, the lifetime of organic dyes is much less than 20 years, during which the initial power of silicon solar modules is reduced to
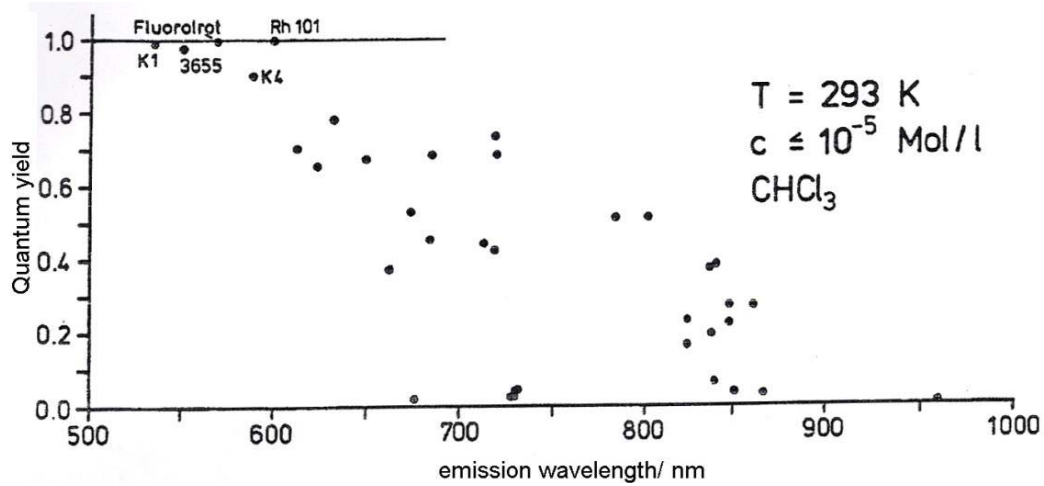
Fig. 8. Quantum yield of the dye as a function of the emission wavelength [12].

80% [26]. To convert solar energy into electricity, high chemical stability of the luminophore to ultraviolet exposure is required. However, under UV irradiation dyes decompose, and, to prevent degradation of dyes, a filter that eliminates the ultraviolet photons is necessary.

Therefore, the advantages of using dyes include: 1) A large number of different dyes available allows to find the one which luminescence band is in the desired spectral range. 2) The internal quantum yield is high and usually reaches 90…100% for dyes that emit photons in the visible range of the solar spectrum. 3) Transparent polymer plates (such as, *e.g.*, PMMA) can be easily doped with organic dyes.

The main disadvantages of dyes are: 1) Concentration quenching the luminescence prevents using high concentration of the dye in the transparent matrix. 2) The light absorption in the dyes occurs in bands of limited width. 3) Most of the dyes are not sufficiently stable, and particularly strong degradation of their properties takes place under the ultraviolet light. 4) A significant overlap of the absorption and luminescence spectra causes significant losses of luminescence quantum due to their reabsorption. 5) The plate doped with the dyes must have a significant thickness to maximize light absorption. 6) The dyes have a low luminescence quantum yield in the infrared range.

4.3. Quantum dots

Quantum dots (QDs) are nanocrystalline particles with their size comparable or less than the Mott exciton diameter. The size of semiconductor QD nanoparticles lies typically in the range of 1 to 20 nm. In these QDs, the energy of electrons and holes are quantized. This results in formation of the large number of quantized levels in the allowed band of energies (Fig. 9 [27, 28]). In the case of strong quantization, when $r < \alpha_e$, α_h (here r is the radius of the nanoparticles, α_e and α_h are the Bohr radius of electron and hole, respectively) the quantized energy levels are:

$$E_{l,n}^{e,h} = \hbar^2 k_{l,n}^2 / 2m_{e,h} ,\tag{5}$$

where $k_{l,n} = \varphi_{l,n}/r$, l is the orbital quantum number, $n = 1,2,3, ...$ – radial quantum number, $\varphi_{l,n}$ – universal series of numbers equal to the serial number of the root of Bessel functions (Table 1 [29]). The value $\varphi_{l,n}$ does not depend of r.

The absorption spectrum of the nanocrystals originates from transitions between the size-quantized levels of electrons and holes with the same quantum numbers n and l (Fig. 9). In this case, the absorption coefficient K depends on the photon energy as [30]:

$$K = A\sum_{l,n}(2l+1)\frac{\mu}{\hbar^2 k_{l,n}^2}\xi_{l,n}^{-3/2}P\left(\frac{r}{\bar{r}}\right),\tag{6}$$

where the constant A is proportional to the square of the matrix element module, $\mu = m_e m_h/(m_e+m_h)$ is the reduced effective mass, $\xi_{l,n} = 2\mu(h\nu - E_g)/\hbar^2 k_{l,n}^2$, $k_{l,n} = \varphi_{l,n}/r$, E_g – bandgap of bulk material, $\bar{r}$ – average radius of nanocrystals, $P(r/\bar{r})$ is the size distribution function of nanocrystals.

Table 1. Roots of the Bessel functions $\varphi_{l, n}$ [30].

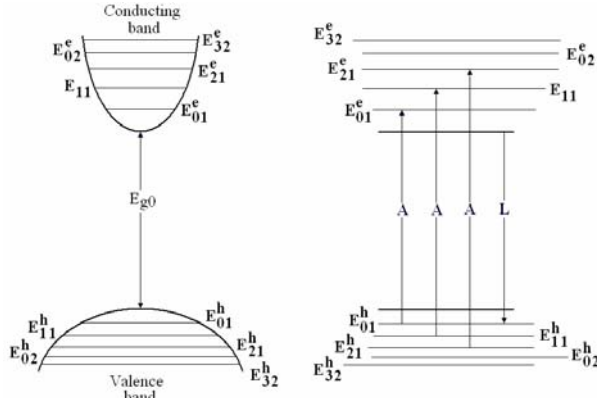| n \ l	1	2	3	4
0	3.142	6.283	9.425	12.566
1	4.493	7.725	10.904	14.066
2	5.764	9.095	12.323	
3	6.988	10.417	13.698	
4	8.183	11.705		
5	9.356	12.967		
6	10.513	14.207		
7	11.657			
8	12.791			
9	13.916			

Fig. 9. The energy spectrum of QD (left) and transitions that form absorption and luminescence spectra (right). E_{g0} is the bandgap of the bulk semiconductor; A and L are transitions that are involved in the absorption and emission of light.

Note that the absorption spectrum of a separate quantum dot contains narrow delta-shaped bands. Due to variation in size of nanocrystals the delta-shaped absorption bands are spread and start overlapping, thus forming a continuous absorption spectrum. Such distribution is typical for any nanocrystal synthesis technology, including the nanocrystals that can be purchased [31]. A typical nanoparticle absorption spectrum is shown in Fig. 10 [32, 33]. According to Fig. 10, changing the size and type of semiconductor nanoparticles allows to control the energy position of the absorption spectrum of quantum dots. It is also seen that apart of some oscillations due to dimensional quantization, quantum dots absorption spectrum resembles spectrum of the bulk semiconductors. Position of the energy absorption bands in nanoparticles can be described by the relation

$$hv^{abs} = E_g^{vol}(abs) + E_q^e + E_q^h = E_g^{vol}(abs) + (\hbar\varphi_{l,n})^2/2m_e r^2 + (\hbar\varphi_{l,n})^2/2m_h r^2 , \tag{7}$$

where $E_g^{vol}(abs)$ is the bulk semiconductor bandgap, E_q^e and E_q^h are the size quantization energy of electron and hole, respectively, m_e and m_h are the effective mass of electron and hole, respectively, r is the radius of nanoparticles, $\varphi_{l,n}$ – constant (for the lowest quantum level $\varphi_{l,n} = 3.14$). Therefore, changing the semiconductor type and QD size, it is always possible to fit the luminescence energy band to the maximum sensitivity of photoconductor.

Luminescence spectra (Fig. 10) are due to electron transition from the lowest electron quantization level to the highest quantization level of hole (Fig. 9). The fluorescent band width is determined by the spread of nanoparticles sizes. Energy position of the luminescence peak can be estimated as follows:

$$hv_{ev}^{PL} = E_g^{PL} + E_q^e + E_q^h - E_{eh} \tag{8}$$

$$hv^{abs} - hv_{ev}^{PL} = E_{eh} = 1.8e^2/4\pi\varepsilon\varepsilon_0\bar{r} \tag{9}$$

where ε and ε_0 are the permittivity of semiconductor and electric constant of vacuum, respectively. According to (6), narrowing the nanoparticle size distribution results in narrowing the luminescence band. Properly choosing the average QD size $\bar{r}$ leads to reduction of the overlap of the absorption and luminescence spectra, which allows reabsorption to be negligible.
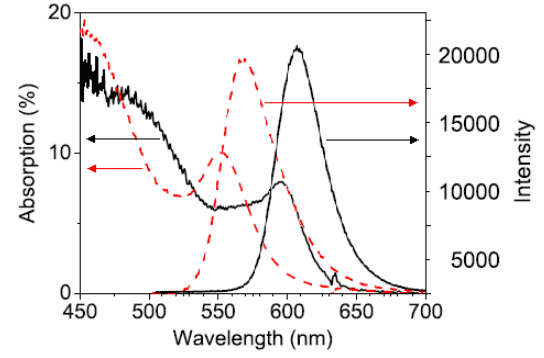
a)
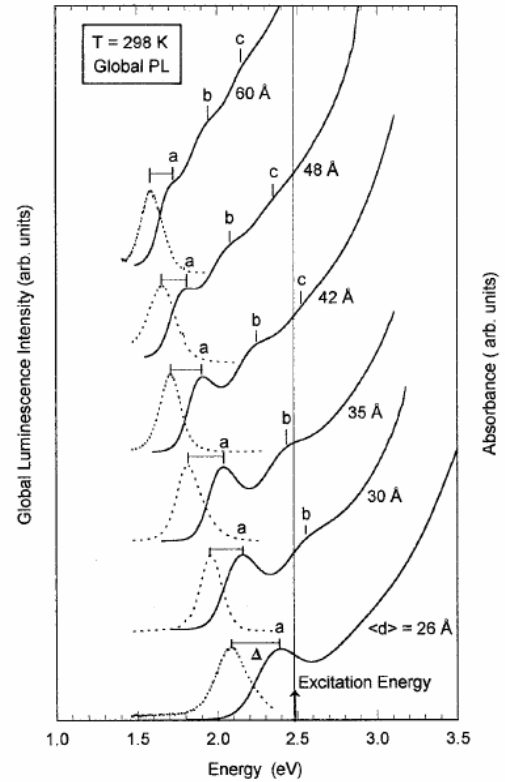
b)

Fig. 10. a) Typical absorption and photoluminescence (PL) spectra of CdSe quantum dots. The thick line represents absorption and photoluminescence spectra of the quantum dots with the mean diameter of 4.3±0.4 nm. The dashed line shows absorption and photoluminescence spectrum from the 3.1±0.3-nm quantum dots. It is clear that the absorption spectrum shifts to the shorter wavelengths for smaller quantum dots [32]. b) Absorption (solid line) and PL (dotted line) spectra at 298 K for colloidal ensembles of InP QDs with different mean diameters. All QD colloidal samples were photoexcited at 2.48 eV [33].

Currently, the results of researches on the single fluorescent quantum dots are available (see, *e.g.*, [34-36]). Specifically, the half-width lines luminescence of the CdSe/ZnS core/shell quantum dots by various estimates [34-36] are within the range from 1.5 to 4.4 GHz or 6.2 to 0.18 μeV. In particular, choosing the optimal synthesis technology of PbSe nanoparticles, their luminescence quantum yield can exceed 80% [37].

We have to note that apart from the exciton bands, the impurity luminescence bands can be present due to presence of the impurity atoms in the bulk of quantum dots or their own defects. By choosing the optimal synthesis technology, one can achieve dominance of the exciton luminescence bands. On the other hand, coating of the quantum dot with shells of the wide gap semiconductor materials followed by deposition of a surface-active layer of organic coating can provide surface passivation of dangling bonds. This alleviates the influence of the non-radiative recombination and prevents coagulation of the quantum dots.

The advantages of QD based luminophores are [38]:

1) Crystalline semiconductor QDs of nanometer size degrade less than organic dyes and their properties can be kept constant throughout the decades.
2) High fluorescence quantum yield in QDs remains at the room temperature. If full passivation of the QD surface is achieved, the internal quantum yield of quantum dots luminescence can be close to unity.
3) The absorption edge of QDs can be adjusted by selecting their diameter.
4) The width of the absorption spectra of QD is large, and it also covers the UV region.
5) When the defects in the bulk and on the surface of the quantum dots are minimized, the exciton band luminescence prevail and radiation in other bands can be ignored. The width of the luminescence spectrum is defined by the QD size distribution, which in turn can be optimized by selecting proper synthesis conditions. Reducing the QD size distribution results in narrowing the width of the exciton luminescence bands. In the absence of such size distribution, the delta-function like band luminescence is expected.
6) The separation of the absorption band and the luminescence bands can be controlled by changing the diameter of the quantum dots. This allows minimizing the reabsorption influence on the efficiency of solar photovoltaics.
7) The emission wavelength of QDs can be adjusted to ensure the maximum sensitivity of the photoconductor.

Disadvantages of luminophores with quantum dots include:

1) Quantum yield of QD is somewhat smaller in comparison with organic dyes.
2) QDs are substantially more expensive as compared to dyes.
3) The overlap of absorption and emission in many QDs is still not negligible.

4) The presence of water and oxygen ions affects on properties of solutions of quantum dots.
5) The toxicity of the QD elements (such as, *e.g.*, lead and cadmium in CdS and PbS QDs) has to be considered.

In conclusion: if QDs with high quantum efficiency (> 0.99) can be inserted in the suitable transparent media, the LSC high efficiency will be achieved.

4.4. Selecting luminophore

To facilitate the choice of the optimal type of luminophores, their comparative characteristics are shown in Table 2. The data presented in this table suggest that preference should be given to the fluorescent quantum dots since this type luminophore allows achieving the maximum efficiency in converting solar energy into electricity.

5. Photon transport losses

For the luminescent photoconverter to work efficiently, it is necessary to minimize losses of quantum luminescence during their transfer from luminophore to the solar cell. These losses are associated with: (1) reabsorption due to overlapping luminescent and absorption bands, (2) due to a possible presence of the surface roughness hub, (3) the presence of the Stokes shift, (4) leakage of the fluorescent photons from the matrix, (5) with the reflection of the light on the input surface of the solar cell. Here, we analyze these losses in details.

Table 2. Properties of luminophores.

Parameter	Rare-earth atoms	Dye	Quantum dot
The shape of the absorption spectrum	Set of narrow lines (line width < 5.10 nm)	Absorption band width of ~300…650 nm	Great extend
The shape of the spectrum of luminescence	One or more line widths of < 5 nm	Luminescence band width of ~100 nm	Wide band ~50 nm (with a standard synthesis technology).
Luminescence quantum yield	Low ~30…40% for > 800 nm.	~100% in the visible spectrum < 40% for > 800 nm.	More than 80%
Reabsorption	Absent	Large	Significant at standard synthesis technology
Spectral agreement with solar cell	Difficult to implement	Easily to implement	Easily to implement
Stability properties	Sustains over hundreds of years	Sustains for several years	Sustains for several decades
The cost of manufacturing technology	High	Low	Medium

5.1. Reabsorption [9, 14, 39]

In dyes and quantum dots (with a large spread of the nanocrystal sizes), there is overlap of absorption and luminescence spectra, which causes the reabsorption of the luminescence quanta. At each act of reabsorption and appropriate reradiation, a part of photons is lost and this results in decrease of the quantum yield. Relation between the number of reabsorption and reradiation acts j and the quantum efficiency losses as a result of this process is

$$\eta_{a-r} = (\eta_L)^j, \tag{10}$$

where η_L is the luminescence quantum yield. For example, if $\eta_L = 0.95$, after 5 reabsorption-reradiation acts ($j = 5$) $\eta_{a-r} = 0.77$.

Therefore, only when the overlap of the absorption and luminescence spectra is not available, we can neglect the losses of the luminescence quanta caused by the reabsorption and reradiation processes.

5.2. The losses due to leakage

Each luminescent center emits photons isotropically. Among all the angles that the fluorescent photons are distributed, there is a critical angle $\beta_{\tilde{N}}$, equals to the angle of the total internal reflection

$$\beta_{\tilde{N}} = \arcsin(n_s/n_m), \tag{11}$$

where n_s and n_m are the index of refraction outside the plate and of the concentrator plate material, respectively. If the plate is surrounded by air, then $n_s = 1$.

If propagation angles of the luminescence photons $\beta > \beta_{\tilde{N}}$, then due to the total internal reflection the photons are back into the hub plate. After a several reflections from the concentrator surfaces, the photons reach the input surface of the solar cell without losses, *i.e.*, the fluorescent photons propagate in the plate as in an optical waveguide. Total internal reflection defines waveguide properties of the plate luminescence concentrator. However, in very thin plates as a result of interference luminescence quenching can occur. Description of the plane wave propagating inside an infinite waveguide layer can be found in many monographs (see, *e.g.*, [41, 42]).

The energy of the photons that reach the solar cell is converted into the electrical energy. Thus, the concentrator can be considered as a transformer of the broadband short-wave light into a narrow spectral interval, energy location of which coincides with the range of maximum sensitivity of the solar cell. It also serves as a concentrator for collecting the light that falls onto a large area of LSC input and sends it to a much smaller area of the solar cell. In fact, the main characteristic of the fluorescent photoconverter is the efficiency η_{LSC} of conversion of the energy of solar photons into electrical energy.

If the angles of propagating luminescence photons $\beta < \beta_{\tilde{N}}$, the luminescent quanta leave the concentrator (see Fig. 3). The amount of these losses can be estimated using the formula [14]

$$\eta_w = \frac{\sqrt{n^2 - 1}}{n}. \tag{12}$$

Specifically for plates with a refractive index $n = 1.5$, which are doped with luminophore, the luminescence quanta that escape through the cone towards the top of the concentrator plate is ~12.5%. The same number of the luminescence photons leaves the plate through its bottom surface.

The total internal reflection is a process without loss of luminescent photons. However, the surface of the luminescent concentrator is not perfect. The presence of roughness on the surface causes the light scattering, which also contributes to the losses. Also, a contamination of the plate can seriously affect the efficiency of the light waveguide.

The easiest way to reduce the leakage losses is to use a filter that reflects escaping light back to the plate solar concentrator (Fig. 11), thus reuse this light. Reflection coefficient of the filter should be close to 100%, however it should reflect the fluorescent photons in the plate and transmit the incoming photons of the lower and larger energy light quanta (Fig. 12). The multilayer interferential filters can be used for this, and when using these filters one has to consider the following issues.
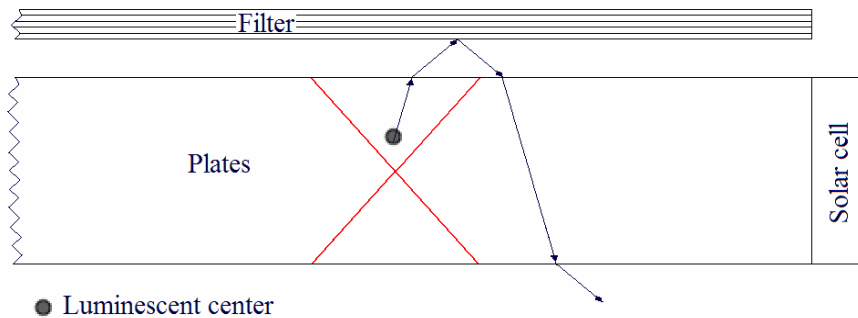

Fig. 11. Illustration of a narrow-band interferential filter. Luminescence photons contained within the cone escape through the upper surface of the plate and are reflected back to the plate, pass through the plate and escape through the bottom surface.
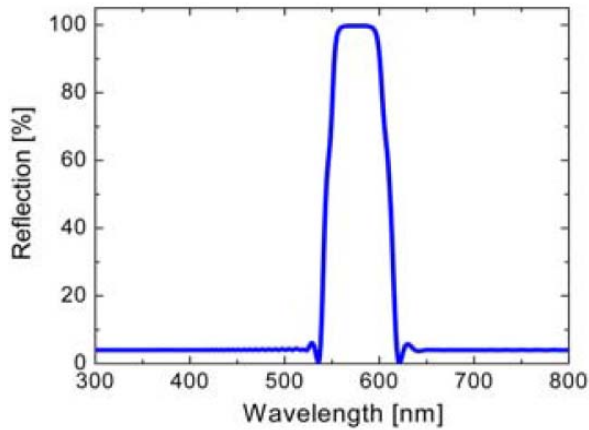
Fig. 12. Calculated reflection spectrum of an optimized Rugate filter. This filter shows only a single reflectance peak and very low reflection otherwise [9].

1) Luminescence quanta propagating in the concentrator plate at larger than critical angles can be reflected from the face and back surface of the plate rather (hundreds of times) before they reach the surface of solar cell.

2) The reflection bandwidth and its energy position depend on the angle of incidence (Fig. 13 [42]). To minimize the losses of fluorescent photons caused by the light falling onto the surface of the filter at different angles the refractive index of the plate material should be as high as possible.

3) Since the coefficient of reflection for the interference filter is always slightly less than unity, if the reflection coefficient is 99%, the percentage of photons which are left behind, for example, 100 reflections should be $0.99^{100} = 0.36$, which is 36%. If reflection of the fluorescent quanta is due to the total internal reflection, 100% of the reflected photons remain. This means that between the plate and interference filter an air gap is required.

4) We have also to remember that the rays reflected by the filter propagate in plate under the same angles, under which they come out of the plate. This means, if it has only the upper interference filter, then all light propagating within the cone passes through the plate. In the presence of filters located on face and back surface of the plate, fluorescent photons within the cone are completely lost due to absorption in the matrix (in the absence of reabsorption).

5) The losses increase significantly when reabsorption is available, because after each act of absorption there is lost 25% of fluorescent quanta emitted inside the cone towards the face and back surfaces of the plate.

Therefore, to minimize leakage losses, reflector should be separated from the plate luminescent concentrator, and not put it directly on the surface of the plate luminescent concentrator. Light, which comes out from the back surface, should be used to excite the luminophore in the plate, which is located under this plate.

5.3. Losses due to reflection of the input surface of the solar cell

In the luminescent concentrator, the solar cells are optically related with the concentrator. If the fluorescent quanta fall onto the solar cell face, a part of them is reflected from the cell face. To reduce these losses, the incoming surface of cells is made as a set of small pyramids, and the antireflecting layer is deposited on the surface of pyramids, it is usually silicon oxide. As a result, the losses caused by reflection become negligible.

5.4. Losses due to the light absorption in the material plate

The plate concentrator should satisfy the following requirements [12]:

1. To be transparent to light of AM0 and AM1.5 spectra, that is to have close to 100% optical transparency in the visible and near infrared regions.
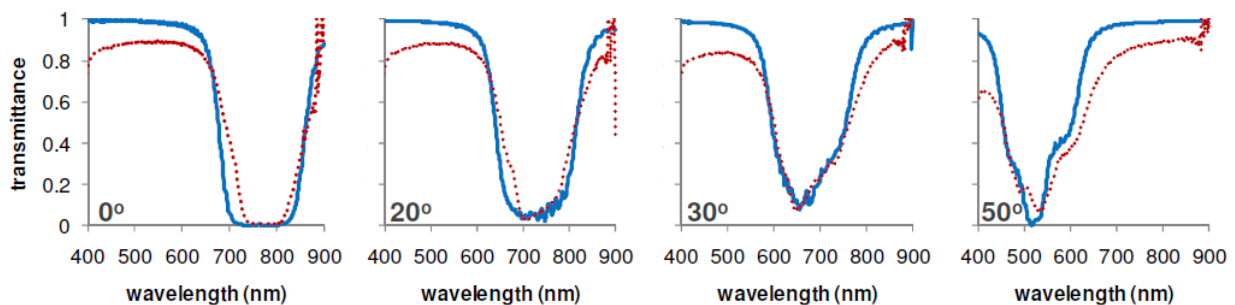

Fig. 13. Transmission spectra for various angles of incidence (in glass) of a right-handed cholesteric liquid crystals (CLC) stacked on the top of the left-handed CLC. The pitch varies linearly from 437 up to 520 nm in the right-handed material and from 429 up to 521 nm in the left-handed material, respectively. Dashed lines indicate the experimental data, solid lines indicate simulated results (taken from [42]).

2. To allow doping of the plate, which provides absorption of all light quanta in the required spectral range $Kd \geq 5$.
3. Doping the plate with luminophore should not reduce the internal quantum yield of luminescence. It should be maximized (preferably equal to unity).
4. To be chemically stable, ideally inert.
5. To have sufficient flexibility, *i.e.*, the ability to easily form plate of a given shape.
6. To be mechanically robust, the big plate of luminescent concentrator should withstand its own weight.
7. The matrix photostability must be high and not change significantly over 20…25 years, *i.e.*, during the warranty period of solar panels.
8. To have a high resistance to atmospheric influences (temperature fluctuations, wind, oxidation), ideally within 20…30 years, *i.e.*, during the solar cells lifespan.
9. To have a low density of the plate material, preferably < 1 g/cm^3, so that the plate of 100 cm×100 cm×1 cm dimension has the weight < 10 kg.
10. To be cost-efficient.
11. To have zero toxicity.
12. To have a high refractive index, required disclosure to minimize light leakage from the cone.
13. Additional requirements for photovoltaic LC matrix for space application are the stability of matrices with respect to the radiation damage.

Most of these requirements are met by silica, glass, and transparent organic plastics. The following properties of silica are attractive for the matrix. This material is transparent within the spectral region 0.2…3 mm (Fig. 14 [43]). The absorption coefficient of the silica plates in this spectral region is very small. For example when $\lambda = 1$ µm $K = 1 \cdot 10^{-5}$ cm^{-1} [45]. The melting point of silica is 1730 °C [44].

Another material that can be used to manufacture the plate concentrator is glass. Among all glasses [45], the most promising is borosilicate glass, particularly N-BK7 type of the glass. The range of transmission for this glass is shown in Fig. 15 [46]. The absorption coefficient of this glass within the spectral range 370 to 1500 nm is less than 0.01 cm^{-1} [45]. Borosilicate glass melting temperature depends on the composition and lies in the range 1200…1500 °C [47].

Optically transparent polymers can be also used to produce fluorescent concentrator plates. They are: polymethyl methacrylate (PMMA), polyvinyl chloride (PVC), polyethylene terephthalate (PET), and polycarbonate (PC). Fig. 16 shows the transmission range of some of these materials. It can be seen that the difference between the transmission spectra of these materials is negligible. However, in experimental researches of the properties of luminescent concentrators polymethyl methacrylate (organic glass) is mainly used. It shows the average value of the absorption coefficient of organic glass in the visible spectrum, which is about

0.001 cm^{-1}. The mixture of luminophore (rare-earth atoms, dyes, quantum dots) with monomer PMMA can be polymerized at the temperatures of 140 °C $< T <$ 170 °C [48]. These temperatures do not affect the properties of organic dyes and the shell quantum dots.

So, among all the materials suitable for manufacturing plate concentrator, preference should be given to organic glass.
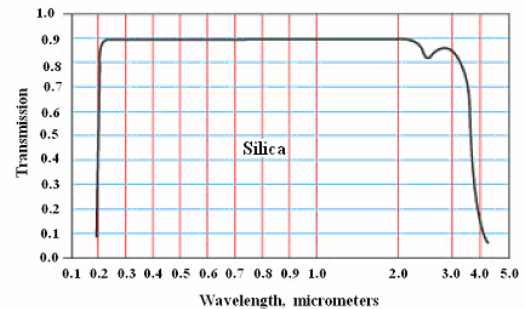

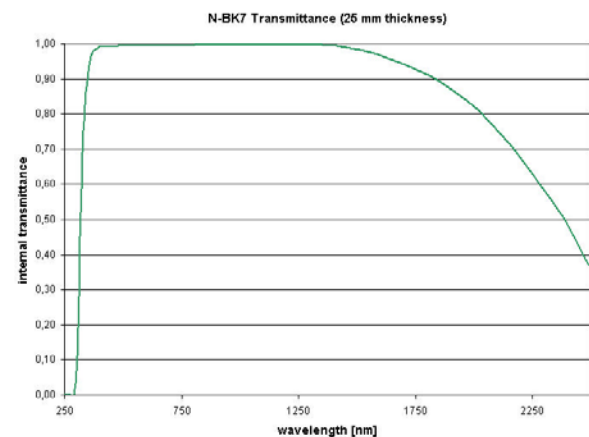**Fig. 14.** The transmission spectrum of silica [43].

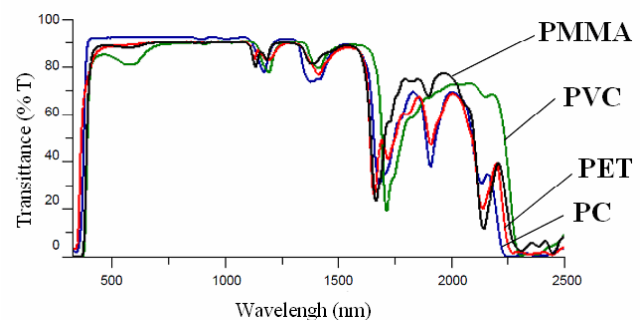**Fig. 15.** The range of internal transmittance for the N-BK7 glass (taken from [46]).

Fig. 16. Transmission spectra of various plastic plates (thickness of 2 mm). Various plastic materials: polymethyl methacrylate (PMMA), polyvinyl chloride (PVC), polyethylene terephthalate (PET), and polycarbonate (PC) – were analyzed, and their transmission spectra are shown in this figure. It was found that the transmittance differs depending on material [48].

6. Design of fluorescent photoconductor

Consideration of the fluorescent concentrator design includes selection of the geometric dimensions of the plate concentrator, analysis of manufacture technology suitable to form the stacked concentrators and attaching the solar cells to the fluorescent concentrator, in particular electrical connection of solar cells.

6.1. Influence of collector geometry

In the research of the fluorescent concentrator properties, the plates are often made in shape of a quadrangle, although they can be made in various shapes: triangle, square, semi-circle [12]. The shape of the plate influences on the uniformity of illumination of the end surfaces. Best lighting uniformity at the end can be achieved with a circular form since the light is completely symmetrical. Assuming that the efficiency of the solar cells has its highest value when they are made of monocrystalline materials and have the form of plates, the best compromise is to manufacture the concentrator plates in the form of hexagonal prisms (Fig. 17).
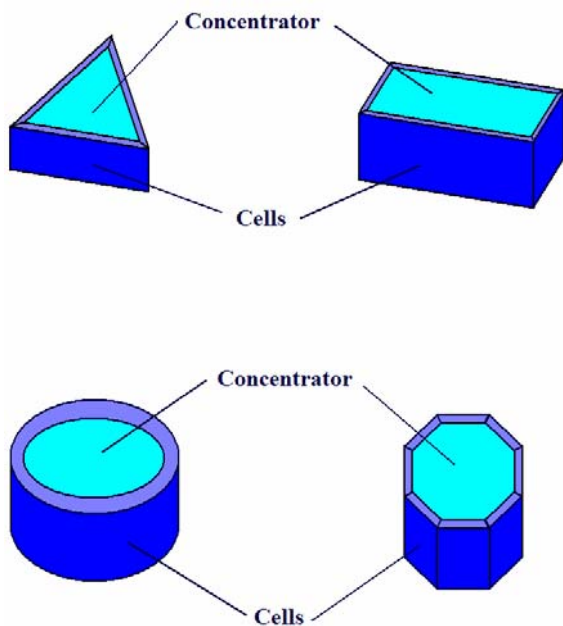

Fig. 17. Possible shape of luminescent concentrators with attached solar cells

The plate thickness should be chosen to fully absorb the light by luminophore, it is sufficient when $Kd = 5$. We assume that the light is fully absorbed by the luminophore with $K = 10$ cm^{-1}, and in this case, $d = 0.5$ cm. Typically, the plate thickness is within the range of 0.2…0.5 cm and the sheet material (PMMA) can be easily formed with this thickness. Too thin plates are not strong enough to support the LSC. Conversely, a thicker sheet will increase the weight of the LSC, which is also not desirable. Therefore, we further assume that $d = 0.5$ cm.

In the absence of reabsorption, other geometric concentrator dimensions define the absorption coefficient of the matrix and the maximum part of luminescent photons. For example, we define the geometric parameters of the rectangular hub based on PMMA.

Consider that the luminescent center is located in the lower corner of the plate (Fig. 18). The longest path is inherent to the beam originating from this center for the angle equal to the angle $\beta_{\tilde{N}}$ of the total internal reflection. If on this path the loss of luminescence quanta caused by light absorption in the matrix does not exceed 10%, then by the end of the path 90% of the quantum luminescence will be available.

It means that in the PMMA plate with the absorption coefficient 0.001 cm^{-1} in the visible spectral region, the longest path for the luminescent photons should not exceed ≈ 2300 cm. At the wavelength of 900 nm, the absorption coefficient in plexiglas is 0.05 cm^{-1}. In this case, the maximum length of the luminescence quantum propagation should not exceed 46 cm. Then, one can calculate the length L_S and area S_S of the side face. For the plates with the absorption coefficient $K_m = 0.001$ cm^{-1} and $K_m = 0.05$ cm^{-1}, the calculated L_S values are equal to 1430 and 28.6 cm, accordingly, and S_S equals to 715 and 14.2 cm^2. Finally, we find the correspondent entrance area that equals to 4293184 and 818 cm^2. Finally, we calculate the maximum gain, which equals to 6004 and 57, respectively.

6.2. The design of the stacked photoconverter

Fig. 19 shows one of the possible stacked concentrator designs. The structure is a combination of interference filters and fluorescent concentrators with the solar cells
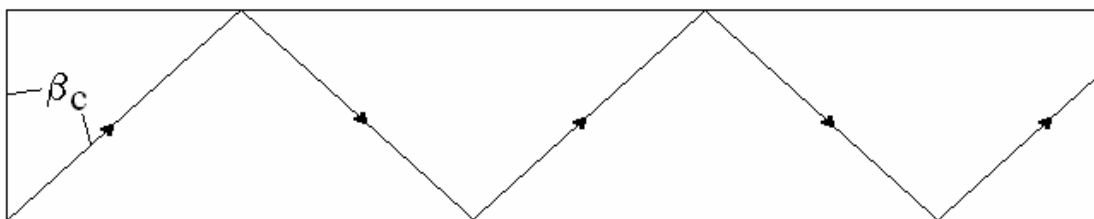

Fig. 18. The schematic distribution of fluorescent photons, used to calculate the geometric dimensions of the concentrator.

attached to the plate. The thickness of the plates and filters should be such to avoid deformation due to its own weight. The air space should be present between the filters and plates,. First, it is necessary to implement the total internal reflection of the luminescence photons emitted and then transported to the solar cell. Second, the filter returns luminescent quanta that escape the cone in the plate. To minimize the losses, the reflection coefficient of the filter should be close to 100%. Third, the filter transmittance must be also close to 100% for the rest of sunlight. Since the above values cannot be 100%, a part of the luminescent quanta is lost.

Reduction of the above losses can only be achieved using the narrow band luminescence and, therefore, narrow band reflection filter. It means that preference should be given to luminophore with a narrow bandwidth of luminescence and wide spectral range, within which light quanta are completely absorbed by the luminophore. Only quantum dots with minimal sizes can satisfy this requirement.

The disadvantage of the filters is the dependence of the energy position of the reflection band on the angle of incidence of the sunlight onto plate. It means that to form the plates, it is necessary to choose materials with the highest refractive index, which decreases the aperture of the escape cone. Another negative factor is that the tracking systems of the sun position are necessary.
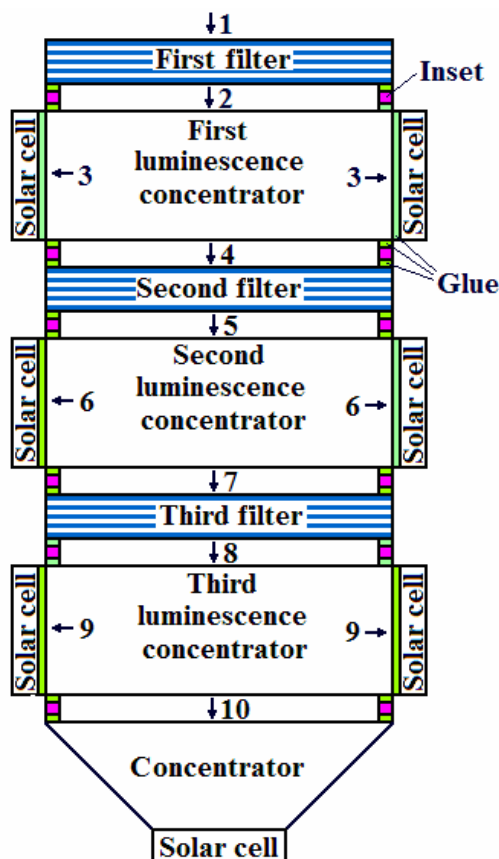

Fig. 19. Schematic diagram of the stacked photoconverter design.

The second concentrator is attached to the first one, and the design elements are repeated. The third last concentrator is attached to the second one with the number of the same design elements. The last plate is different, since it contains the attached lens or non-imaging concentrator and solar cell.

One can use any glue or adhesive to attach the filter to the plate. Information about the properties of the glue and adhesives can be found, for example, in the monograph [49]. To attach the solar cell to the plate, one can use any glue, which is transparent in the visible and infrared regions. Information about the properties of this glue one can found, for example, in the monograph [50]. In the spectral band 320 to 2700 nm, Canadian balsam is often used as optically transparent adhesive. If Canadian balsam is 0.01-mm thick, then its transmission exceeds 99% [50].

Fig. 20 shows evolution of the light in the photo-converter. At the top of stacked fluorescent concentrators, the filter is placed. Let normally incident sunlight (for the sake of being specific, AM1.5) illuminates the plate. The filter reflects luminescent quanta (Fig. 20-1), which are emitted by the luminophore of first concentrator in a narrow band. The filter reflection coefficient should be close to 100%. Transparence in a low and a high energy bands should be close to 100%.

Light that passes through the first filter (Fig. 20-2) enters to the first plate (for certainty, plate of PMMA). High-energy light is absorbed by the luminophore that generates luminescent quanta in the narrow band. Approximately 82.5% of the luminescence quanta is transported to solar cells attached to the first concentrator plate (Fig. 20-3).

To avoid the losses of light during its transport to the cells the gap should introduced between the filter and plate. Approximately 12.5% of fluorescent photons propagates toward the filter that reflects it back to the plate. The photons passing through the plate without absorption travel toward the second filter. In the same direction, 12.5% of fluorescent photons travels, which are emitted in the first plate within the critical cone (Fig. 20-4).

Next, on the second filter 12.5% fluorescent photons falls, which are emitted by quantum dots in the first plate as well as rest sunlight. The second filter reflects light in a narrow spectral range (Fig. 20-5), which is emitted in the luminescence band of luminophore of a second plate. Approximately 87.5% of fluorescent quanta are transported to solar cells attached to the plates of the second plate (Fig. 20-6). The fluorescent photons out of the second plate and rest sunlight photons fall onto the third interference filter (Fig. 20-7). This filter reflects luminescent quanta contained in the third plate (Fig. 20-8). Approximately 87.5% of fluorescent quanta are transported to solar cells attached to the third plate (Fig. 20-9). Rest of fluorescent photons goes out of the third plate (Fig. 20-9), and the rest of sunlight is transported by non-imaging concentrator directed to the solar cell (Fig. 20-10).

7. Discussion

The main purpose of this work is to predict the properties of the solar cells with the fluorescent concentrators and to identify the factors, the implementation of which ensures maximum efficiency of converting solar energy into electricity. When considering the properties of solar cells, we explicitly or implicitly supposed that they can convert into electrical energy both photons of light directly falling onto the concentrator and the photons of the scattered light. It is also considered that for such solar cells the tracking system is not required.

The key features are photoconverter stacked fluorescent concentrators is that it can use the entire spectrum of solar radiation, which spectrally fits the solar cells. In this case, we have a freedom in choosing the material to produce solar cells, and more freedom in joining the cells.

Usage of the stacked plates can reduce the temperature of the solar cell, since the thermal load occurs in plates, not in the cells. It results in increase of the efficiency of the solar cells.

To minimize the losses caused by leakage, one has to use the interference filters that effectively reflect the flow of escaping fluorescent photons and at the same
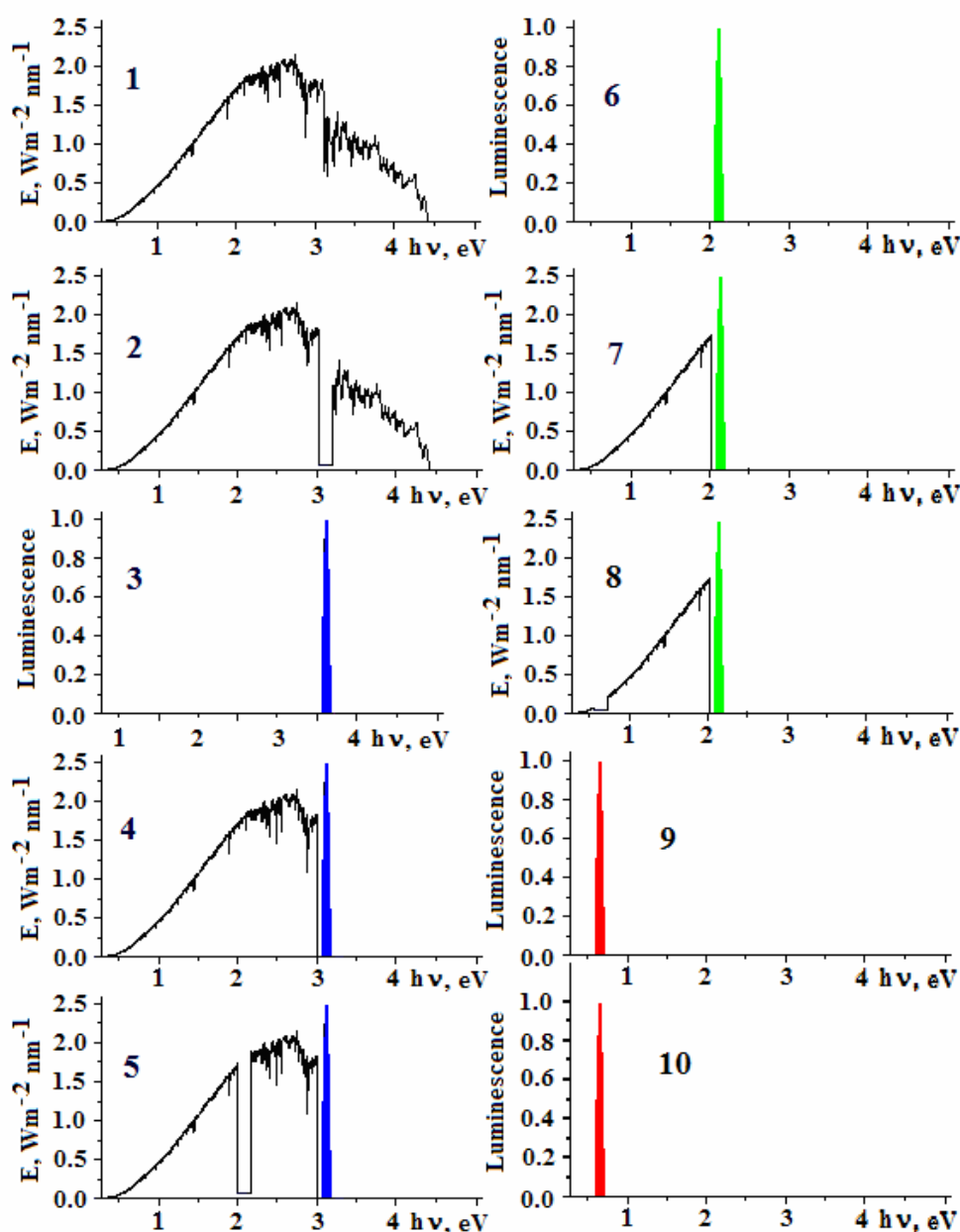

Fig. 20. Evolution of light in its distribution inside solar cells with fluorescent concentrators.

time are transparent for direct sunlight. Sunlight falls onto the filter under large angles to this filter, which requires the tracking systems. Besides, with the presence of filters, the ability to use the diffuse light scattered in all directions from the clouds, trees, variety facilities is lost. Impossibility to use scattered light by filtering systems and need to expend the energy for managing systems following the sun indicate inappropriate development of solar cells with fluorescent concentrators with the band-pass filters introduced to them.

8. Conclusions

Our comparison of the properties of materials suitable for making plates for luminescent concentrators allows us to give a preference to silica, and in assessing the real values of the efficiency – to polymethyl methacrylate.

From a comparison of the properties of such luminophores as ions of rare-earth metals, dyes, semiconductor quantum dots, we can conclude that for the doped concentrator plates the use of the quantum-dimensional nanocrystals is most appropriate.

Inability to use ambient diffuse light to convert its energy into electrical energy and the need to use extra energy for the tracking systems allow us to conclude that the use of the luminescent solar concentrators with the interference filters are not justified.

References

1. O. Semonin, J.M. Luther and M.C. Beard, Multiple exciton generation in a quantum dot solar cell // 26 March 2012, *SPIE* Newsroom. DOI: 10.1117/2.1201203.004146
2. W. Shockley and H.J. Queisser, Detailed balance limit of efficiency of p-n junction solar cells // *J. Appl. Phys.* **32**(3), p. 510-519 (1961).
3. M.A. Green, K. Emery, Y. Hishikawa, W. Warta and E.D. Dunlop, Solar cell efficiency tables (version 43) // *Prog. Photovolt.: Res. Appl.* **22**(1), p. 1-9 (2014).
4. J.F Geisz, S. Kurtz, M.W. Wanlass, J.S. Ward, A. Duda, D.J. Friedman, J.M. Olson, W.E. McMahon, T.E. Moriarty, J.T. Kiehl, High-efficiency GaInP/GaAs/InGaAs triple-junction solar cells grown inverted with a metamorphic bottom junction // *Appl. Phys. Lett.* **91**, No.2, p. 023502 (2007).
5. L. Mearian, New solar cell sets world record, focusing the power of 297 suns // News September 26, 2013 03:53 PM ET; http://*www.computerworld.com/article/*2597774/*emerging-technology/new-solar-cell-sets-world-record-focusing-the-power-of-297-suns.html;* Mark Osborne, Quadruple III-V bonded CPV cell hits 44.7% record conversion efficiency // 24 September 2013, 16:12 In News, Thin Film, III-V; *http://www.pv-tech.org/news/quadruple_iii_v_bon-ded_cpv_cell_hits_44.7_record_conversion_efficiency*
6. A.V. Sachenko, M.R. Kulish, I.O. Sokolovskyi, V.P. Kostylyov, Lateral multijunction photovoltaic cells // *Semiconductor Physics, Quantum Electronics & Optoelectronics*, **16**, No.1, p. 1-17 (2013).
7. M.A. Green and A. Ho-Baillie, Forty three per cent composite split-spectrum concentrator solar cell efficiency // *Prog. Photovolt.: Res. Appl.* **18**, p. 42-47 (2010).
8. Lo Chin Kim, Simulation and construction of luminescent solar concentrator // *A master thesis* submitted to the Department of Electrical and Electronic Engineering, Faculty of Engineering and Science, University Tunku Abdul Rahman, in partial fulfillment of the requirements for the degree of Master of Engineering Science, November 2011, p. 1-262.
9. J.C. Goldschmidt, Novel solar cell concepts // *Dissertation* zur Erlangung des akademischen Grades des Doktors der Naturwissenschaften (Dr. rer. nat.) an der Universität Konstanz Fachbereich Physik, Fraunhofer Institut für Solare Energiesysteme (ISE), Freiburg, September 2009, p. 1-280.
10. L.H. Slooff, E.E. Bende, A.R. Burgers, T. Budel, M. Pravettoni, R.P. Kenny, E.D. Dunlop, A. Buechtemann, A luminescent solar concentrator with 7.1% power conversion efficiency // *Physica Status Solidi* (RRL), **2**(6), p. 257-259 (2008).
11. J. Gutmann, M. Peters, B. Bläsi, M. Hermle, A. Gombert, H. Zappe, J.C. Goldschmidt, Electromagnetic simulations of a photonic luminescent solar concentrator // *Opt. Exp.* **20**, No. S2, p. A157-A167 (2012).
12. T.J.J. Meyer, Photon Transport in Fluorescent Solar Collectors // *Doctoral Thesis*, University of Southampton, School of Engineering Sciences, 2010.
13. G. Dieke, *Spectra and Energy Levels of Rare Earth Ions in Crystals*. Interscience Publ., New York, 1968.
14. L.R. Wilson, Luminescent Solar Concentrators: A Study of Optical Properties, Re-absorption and Device Optimization // *Doctor of Philosophy*. Department of Mechanical Engineering School of Engineering & Physical Sciences, Heriot-Watt University, Edinburgh EH14 4AS, United Kingdom, May 2010.
15. A.K. Gupta and S.K. Ujjwal, Optical absorption spectra of rare earth elements with amino acid in different solvents // *Adv. in Appl. Sci. Res.* **4**(3), p. 33-38 (2013).
16. A.K. Gupta, and S.K. Ujjwal, Absorption spectra of praseodymium with amino acid // *Res. J. Phys. Sci.* **1**(4), p. 7-10 (May 2013).
17. R. Van Deun, P. Fias, P. Nockemann, K. Van Hecke, L. Van Meervelt, and K. Binnemans, Visible-light-sensitized near-infrared luminescence

from rare-earth complexes of the 9-hydro-xyphenalen-1-one ligand // *Inorg. Chem.* **45**, p.10416-10418 (2006).

18. K. Binnemans, P. Lenaerts, K. Driesen and C. Gorller-Walrand, A luminescent tris(2-thenoyltrifluoroacetonato)europium(III) complex covalently linked to a 1,10-phenan-throlinefunctionalised sol–gel glass // *J. Mater. Chem.* **14**, p. 191-195 (2004).

19. X. Zhang, S. Wen, S. Hu, L. Zhang, L. Li, Electrospinning preparation and luminescence properties of Eu(TTA)3phen/polystyrene composite nanofibers // *J. Rare Earths*, **28**, No. 3, p. 333-339 (June 2010).

20. T. Förster, Intermolecular energy migration and fluorescence // *Ann. Phys.* **2**, p. 55-75 (1948).

21. D.L. Dexter, Theory of optical properties of imperfections in nonmetals // *Solid State Phys.* **6** (Eds. F. Seitz and D. Turnbull), p. 353-411 (1958), Academic Press.

22. J.-C.G. Bünzli, S.V. Eliseeva, Lanthanide NIR luminescence for telecommunications, bioanalyses and solar. Review // *J. Rare Earths*, **28**, No. 6, p. 824-842 (Dec. 2010).

23. J.-C.G. Bünzli and A.-S. Chauvin, Lanthanides in solar energy conversion. In: *Handbook on the Physics and Chemistry of Rare Earths*, Eds. J.-C.G. Bünzli and V.K. Pecharsky, Vol. 44. Amsterdam, The Netherlands, 2014, p. 169-281.

24. J.S. Batchelder, The luminescent solar concentrator // *Thesis for the degree doctor of philosophy*. California Institute of Technology, Pasadena, California, 1982, p. 1-287.

25. *Catalogue of Active Laser Media Based on Solutions of Organic Dyes and Related Compounds*, Ed. V.I. Stepanov. Institute of Physics of Academy of Sciences of Byelorussian SSR, Minsk, 1977 (in Russian).

26. Mono Crystalline Silicon PV Module SF-125×125-72-M/L/D // Zhejiang Sunflower Light Energy Science & Technology Co. Ltd. *www.sunowe.com*; Monocrystalline Silicon Solar Module // Eoplly New Energy Technology Co., Ltd *www.eoplly.com*; Supplementary Warranties Applicable to Bosch Solar c-Si Series of Photovoltaic Modules Supplied by Robert Bosch (Australia) Pty Ltd in Australia after 1st January 2012 // *www.bosch-solarenergy.com.au*.

27. N.R. Kulish, V.P. Kunets, M.P. Lisitsa, N.I. Malysh, Evolution of absorption spectra when transferring from bulk to quantum-sized crystals CdS_XSe_{1-X} // *Ukrainskii Fizicheskii Zhurnal*, **37**, №8, p. 1141-1146 (1992), in Russian.

28. N.R. Kulish, V.P. Kunets, M.P. Lisitsa, Optical properties of quasi-zero-dimensional CdS_XSe_{1-X} crystallites grown in a glass matrix // *Opt. Eng.* **34**, No. 4, p. 1054-1071 (1995).

29. S. Flügge, *Practical Quantum Mechanics*. Springer-Verlag, Berlin – Heidelberg, 1999.

30. A.L. Efros and A.L. Efros, Interband light absorption in semiconductor sphere // *Fizika tekhnika poluprovodnikov*, **16**(7), p. 1209-1214 (1982), in Russian.

31. Nanomaterials and related products catalogue & price-list // *PlasmaChem. Surface and Nano-Technology,* 2014, p. 1-48.

32. A. Irman, Modification of Spontaneous Emission of Quantum Dots by Photonic Crystals // *Graduation Thesis* 11 November 2003. Complex Photonic Systems (COPS) Group MESA+ Institute Faculty of Science and Technology University of Twente, Enschede, The Netherlands. P. 1-48.

33. O.I. Mićic, H.M. Cheong, H. Fu, A. Zunger, J.R. Sprague, A. Mascarenhas, and A.J. Nozik, Size-dependent spectroscopy of InP quantum dots // *J. Phys. Chem. B*, **101**, p. 4904-4912 (1997).

34. S.A. Blanton, M.A. Hines, P. Guyot-Sionnest, Photoluminescence wandering in single CdSe nanocrystals // *Appl. Phys. Lett.* **69**(25), p. 3905-3907 (1996).

35. A.P. Alivisatos, Electrical studies of semiconductor-nanocrystal colloids // *MRS Bulletin*, **23**, Issue 2, p. 18-23 (1998).

36. M.J. Fernée, C. Sinito, Y. Louyer, P. Tamarat and B. Lounis, The ultimate limit to the emission linewidth of single nanocrystals // *Nanotechnology*, **24**, 465703 (5p.) (2013).

37. H. Du, C. Chen, R. Krishnan, T.D. Krauss, J.M. Harbold, F.W. Wise, M.G. Thomas, and J. Silcox, Optical properties of colloidal PbSe nanocrystals // *Nano Lett.* **2**, No. 11, p. 1321-1324 (2002).

38. B. Norton, P.C. Eames, T.K. Mallick, Ming Jun Huang, S.J. McCormack, J.D. Mondol, Y.G. Yohanis, Enhancing the performance of building integrated photovoltaics // *Solar Energy*, **85**, p. 1629-1664 (2011).

39. S. Peeters, Reabsorption Losses in Luminescent Solar Concentrators // *Masterproef* ingediend tot het behalen van de academische graad van Master in de ingenieurswetenschappen: fotonica Academiejaar 2010-2011. P. 1-72.

40. N.J. Cronin, *Microwave and Optical Waveguides*. CRC Press, 1995.

41. R.R.A. Syms and J.R. Cozens, *Optical Guided Waves and Devices*. McGraw-Hill, 1992.

42. D.K.G. de Boer, D.J. Broer, M.G. Debije, W. Keur, A. Meijerink, C.R. Ronda, and P.P.C. Verbunt, Progress in phosphors and filters for luminescent solar concentrators // *Opt. Exp.* **20**, No. S3, p. A395-A405 (2012).

43. *International Crystal Laboratories*. Optics & Spectroscopy Supplies & Accessories. Tel. (973) 478-8944. Fax. (973) 478-4201.

44. Fused Silica (FS) // Del Mar Ventures. 4119 Twilight Ridge, San Diego, CA 92130, tel: (858) 876-3133, fax: (858) 630-2376, *optics@sciner.com, http://www.sciner.com/Opticsland.*

45. Optical glass/ Data sheet // Schott North America, Inc. Advanced Optics. 400 York Avenue Duryea, PA 18642 USA/ *info.optics@us.schott.com*; *www.us.schott.com*.

46. TIE-35: Transmittance of optical glass // October 2005. Optics for Devices SCHOTT North America, Inc. 400 York Avenue Duryea, PA 18642 USA, E-mail: *sgt@us.schott.com*; *www.us.schott.com/ optics_devices*

47. H. Cao, J.W. Adams and P.D. Kalb, Low Temperature Glasses for Hanford Tank Wastes // *Annual Report. FY 1995.* Environmental Sciences Department Brookhaven National Laboratory Brookhaven Science Associates Upton, Long Island New York, 11973, Under Contract No. DE-AC02-98CH10886 with the UNITED STATES DEPARTMENT OF ENERGY.

48. Measurement of Optical Characteristic of Plastic by UH4150 Spectrophotometer. An example of High Throughput measurements in the UV, Visible and Near-Infrared Regions // *Hitachi High-Technologies Corporation*.

49. D.W. Swanson, J.J. Licari, *Adhesives Technology for Electronic Applications – Materials, Processing, Reliability. Materials and Processes for Electronic Applications.* Elsevier Science, August 2005.

50. *Handbook for designer of optical-and-mechanical devices* / V.A. Panov, M.Ia. Kruger, V.V. Kulagin et al. Mashinostroenie, Leningrad, 1980 (in Russian).